

## Vesicle and Stable Monolayer Formation from Simple “Click” Chemistry Adducts in Water

Santanu Bhattacharya<sup>\*,†,‡,§</sup> and Joydeep Biswas<sup>†</sup><sup>†</sup>Department of Organic Chemistry, Indian Institute of Science, Bangalore 560 012, India, and <sup>‡</sup>Chemical Biology Unit of JNCASR, Bangalore 560 064, India <sup>§</sup>J.C. Bose Fellow, DST, New Delhi, India

Received May 28, 2010

Click chemistry has been successfully extended into the field of molecular design of novel amphiphatic adducts. After their syntheses and characterizations, we have studied their aggregation properties in aqueous medium. Each of these adducts forms stable suspensions in water. These suspensions have been characterized by dynamic light scattering (DLS) studies and transmission electron microscopy (TEM). The presence of inner aqueous compartments in such aggregates has been demonstrated using dye (methylene blue) entrapment studies. These aggregates have been further characterized using X-ray diffraction (XRD), which indicates the existence of bilayer structures in them. Therefore, the resulting aggregates could be described as vesicles. The temperature-induced order-to-disorder transitions of the vesicular aggregates and the accompanying changes in their packing and hydration have been examined using high-sensitivity differential scanning calorimetry, fluorescence anisotropy, and generalized polarization measurements using appropriate membrane-soluble probe, 1,6-diphenylhexatriene, and Paldan, respectively. The findings of these studies are consistent with each other in terms of the apparent phase transition temperatures. Langmuir monolayer studies confirmed that these click adducts also form stable monolayers on buffered aqueous subphase at the air–water interface.

## 1. Introduction

Copper(I)-catalyzed cycloaddition between an alkyne and an azide is popularly known as “click chemistry”.<sup>1–3</sup> Click chemistry has been introduced by Sharpless, and it describes a step that is tailored to generate adducts quickly and reliably by joining suitable molecular units together. This is inspired by the fact that nature also generates larger molecules by joining small molecular units. Click chemistry has already found widespread use in diverse fields such as bioconjugation of oligonucleotides,<sup>4</sup> glycoclusters syntheses,<sup>5</sup> design of enzyme inhibitors,<sup>6</sup> and even in polymer and materials science.<sup>7</sup> Further this reaction has been adapted to join lipids with proteins<sup>8</sup> and used to generate synthetic analogues of a type of lipids that occur in archaeobacteria.<sup>9</sup> However, so far there has been no attempt to exploit this useful chemistry for the design of amphiphilic systems that would aggregate in aqueous media to produce nanoscopic ensembles.

Here we present four novel adducts (Figure 1) synthesized using click chemistry: an appropriately chosen monomer (**M1**) along with a dimer (**D1**) and a tetramer (**T1**). A long-chained variant, **M2** of the monomer, **M1**, was also prepared for comparison. The syntheses of **M1**, **M2**, **D1**, and **T1** were accomplished by click

coupling between each of the corresponding propargylated ester precursors and appropriate either mono-, or di-, or tetra-azides, respectively (Schemes 1 and 2). Since these compounds were synthesized by click chemistry, they are exclusively made up of 1,4-substituted 1,2,3-triazoles. In the present set of adducts, appropriate alkyl groups replace the tautomeric H-atom of the triazole backbone. It occurred to us that since the triazoles are significantly polar,<sup>10</sup> the same part of the adduct molecules would get hydrated preferentially than their hydrophobic segments if brought into contact with water. On the basis of the published reports<sup>11</sup> on the basicity constant for *N*-methyl-1,2,3-triazole, each adduct described herein should remain mainly protonated in water at pH ≤ 3.0, as shown in Chart 1.

Upon brief sonication each of these adducts formed stable suspensions in aqueous medium, which were characterized by dynamic light scattering (DLS) studies and transmission electron microscopy (TEM) to determine the average sizes of the aggregates. Such aggregates were found to possess inner aqueous compartments as evidenced from dye entrapment studies, indicating that these adducts on dispersal in aqueous media afforded vesicles. Cast films formed from each of these aggregates were also characterized by X-ray diffraction (XRD) studies, which indicate the formation of a tilted bilayer type arrangements from the aggregates of **M1** whereas regular bilayer structures were predominant from the aggregates derived from each of **M2**, **D1**, and **T1**. The temperature-induced order-to-disorder transitions of the vesicles and the accompanying changes in packing and hydration were examined using high-sensitivity differential scanning calorimetry (DSC), fluorescence anisotropy, and generalized polarization measurements using a membrane-soluble probe, DPH, and a polarity

\*Corresponding author: e-mail sb@orgchem.iisc.ernet.in; Ph (91)-80-2293-2664; Fax (91)-80-2360-0529.

(1) Kolb, H. C.; Finn, M. G.; Sharpless, K. B. *Angew. Chem., Int. Ed.* **2001**, *40*, 2004.

(2) Tornøe, C. W.; Christensen, C.; Meldal, M. *J. Org. Chem.* **2002**, *67*, 3057.

(3) Hassane, F. S.; Frisch, B.; Schuber, F. *Bioconjugate Chem.* **2006**, *17*, 849.

(4) Morvan, F.; Meyer, A.; Pourceau, G.; Vidal, S.; Chevotot, Y.; Souteyrand, E.; Vasseur, J.-J. *Nucleic Acids Symp. Ser.* **2008**, *52*, 47.

(5) Chevotot, Y.; Bouillon, C.; Vidal, S.; Morvan, F.; Meyer, A.; Cloarec, J.-P.; Jochum, A.; Praly, J.-P.; Vasseur, J.-J.; Souteyrand, E. *Angew. Chem., Int. Ed.* **2007**, *46*, 2398.

(6) Srinivasan, R.; Li, J.; Ng, S. L.; Kalesh, K. A.; Yao, S. Q. *Nature Protoc.* **2007**, *2*, 2655.

(7) Binder, W. H.; Sachsenhofer, R. *Macromol. Rapid Commun.* **2007**, *28*, 15.

(8) Musiol, H.-J.; Dong, S.; Kaiser, M.; Bausinger, R.; Zumbusch, A.; Bertsch, U.; Moroder, L. *ChemBioChem* **2005**, *6*, 62.

(9) O’Neil, E. J.; DiVittorio, K. M.; Smith, B. D. *Org. Lett.* **2007**, *9*, 199.

(10) Nulwala, H.; Takizawa, K.; Odukale, A.; Khan, A.; Thibault, R. J.; Taft, B. R.; Lipshutz, B. H.; Hawker, C. J. *Macromolecules* **2009**, *42*, 6068.

(11) (a) Elguero, J.; Katritzky, A. R.; Denisko, O. V. *Adv. Heterocycl. Chem.* **2000**, *76*, 1. (b) Abboud, J.-L. M.; F-Foces, C.; Notario, R.; Trifonov, R. E.; Volovodenko, A. P.; Ostrovskii, V. A.; Alkorta, I.; Elguero, J. *Eur. J. Org. Chem.* **2001**, 3013.

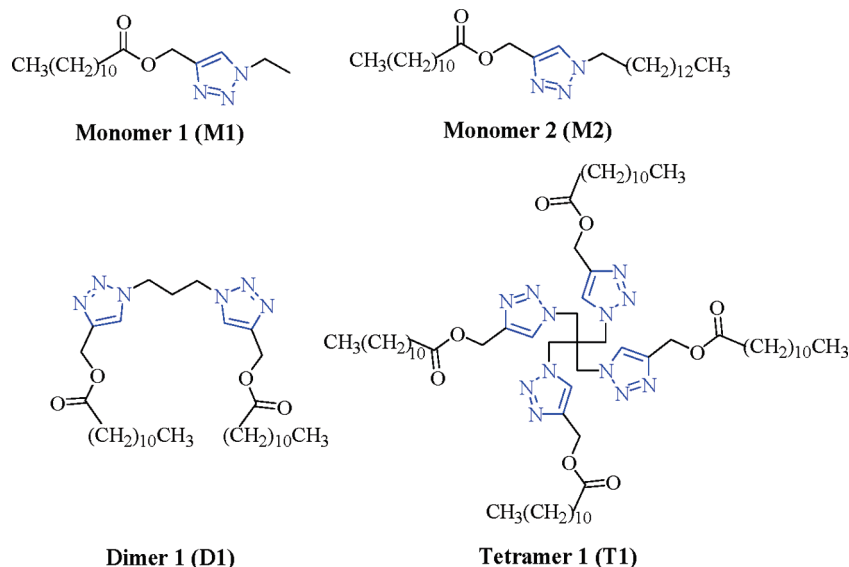
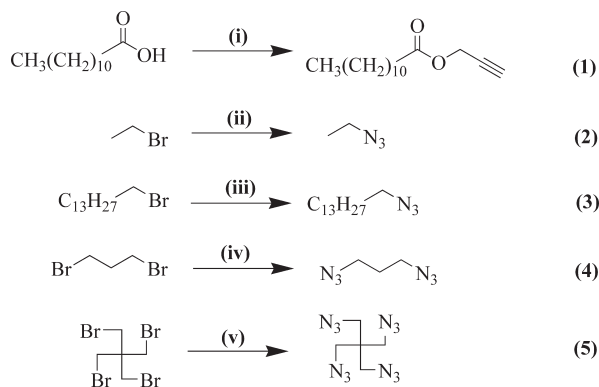


**Figure 1.** Molecular structures of the triazole-based adducts that have been synthesized and used in the present investigation.

#### Scheme 1<sup>a</sup>



<sup>a</sup> Reagents and conditions: (i) DCC, DMAP, THF, rt, 6 h; (ii), (iii), (iv), and (v)  $\text{NaN}_3$ , DMF, 80 °C, 10 h.

sensor, Paldan, respectively. Interestingly, each of these adducts also formed a stable film at the air–water interface as characterized by the Langmuir isotherm studies. Click chemistry thus allows a simple preparation of novel amphiphiles with assorted variation in their head/tail groups and adds to the growing list of new amphiphiles.<sup>12a–f</sup>

## 2. Experimental Section

**2.1. Materials and Methods.** All reagents, solvents, and chemicals used in these studies were obtained from the best known commercial sources. The solvents were dried prior to use. Column chromatography was performed using a 60–120 mesh silica gel. NMR spectra were recorded using a Jeol JNM  $\lambda$ -300 (300 MHz)

for <sup>1</sup>H spectrometer. The chemical shifts ( $\delta$ ) are reported in ppm downfield from the internal standard, TMS, for <sup>1</sup>H NMR. Mass spectra were recorded on a MicroMass ESI-TOF spectrometer. Infrared (IR) spectra were recorded using neat samples on a Jasco FT-IR 410 spectrometer.

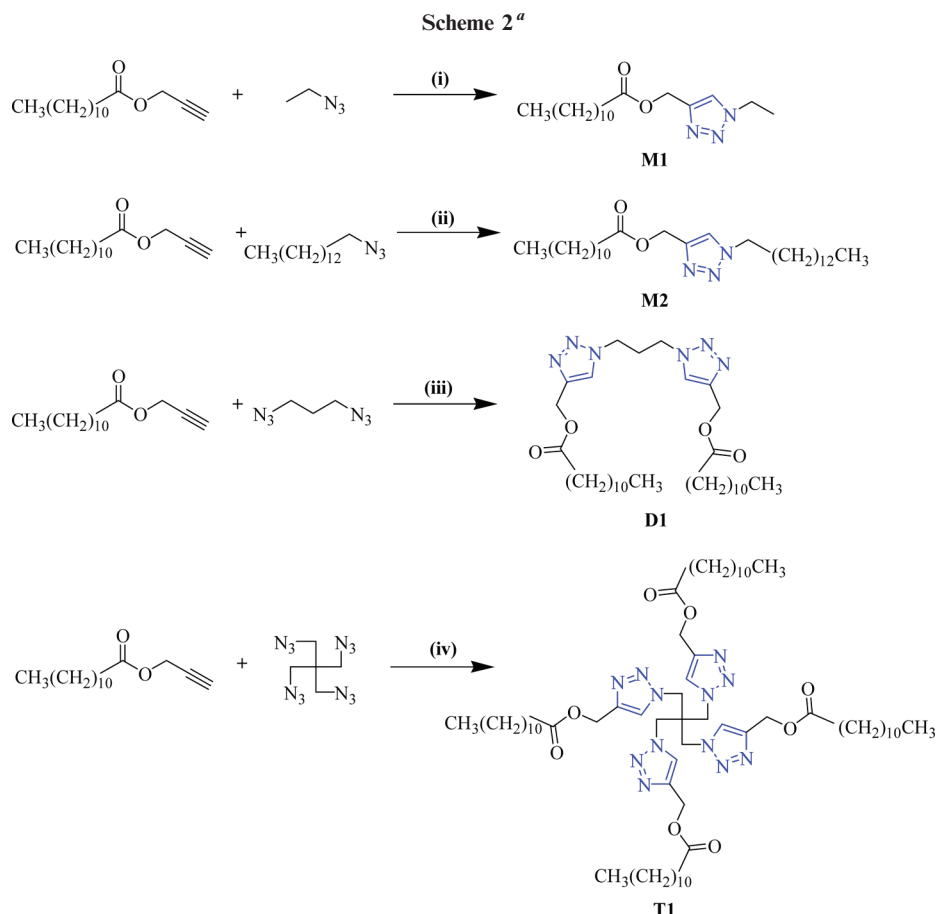
**Caution!** Reactions of azide salts with organic compounds and transformations involving organic azides are potentially explosive. Only small amounts of materials should be used and cautiously handled. Although we did not experience any problem, proper caution must be exercised while handling with all new azide compounds.

**2.2. Synthesis.** *Prop-2-ynyl Dodecanoate (1).* Propargyl alcohol (616 mg, 11.00 mmol) was added to a stirred solution of lauric acid (2.0 g, 10.00 mmol), DMAP (1.59 g, 13.00 mmol), and DCC (2.68 g, 13.00 mmol) in dry THF (12 mL), and the resultant mixture was stirred at room temperature for 6 h. The reaction mixture was then diluted with acetone and filtered. The filtrate was concentrated, diluted with ethyl acetate (50 mL), and washed with saturated aqueous  $\text{KHSO}_4$  solution (20 mL  $\times$  3) followed by water (20 mL) and finally using saturated brine (20 mL). The organic phase was separated, dried over anhydrous  $\text{Na}_2\text{SO}_4$ , and evaporated, leaving a residue. The product residue, prop-2-ynyl dodecanoate (**1**), was found to be of sufficient purity for direct use in the next step without any need for further purification. Yield: light yellow oil, 2.0 g (8.4 mmol, 84.0%). IR (neat) ( $\text{cm}^{-1}$ ): 3313, 2927, 2856, 2131, 1747, and 1158. <sup>1</sup>H NMR (300 MHz,  $\text{CDCl}_3$ ):  $\delta$  0.86 (3H, m), 1.34–1.18 (16H, m), 1.62 (2H, m), 2.36 (2H, t), 2.44 (1H, t), 4.65 (2H, d). ESI-MS calcd. for  $[\text{C}_{15}\text{H}_{26}\text{O}_2 + \text{Na}^+]$ : 261.3555; found: 261.183.

*Azidoethane (2).*  $\text{NaN}_3$  (598 mg, 9.20 mmol) was added to a solution of bromoethane (200 mg, 1.84 mmol) in DMF (5 mL) kept in a screw-top pressure tube, and the resulting mixture was heated to 80 °C for 10 h. Then the solvent was evaporated under vacuum to leave a residue, to which EtOAc was added. This afforded an organic layer, which was washed with water (20 mL  $\times$  2) and followed by saturated brine (20 mL). Because of the potential explosiveness of azides,<sup>13</sup> the organic layer was dried over anhydrous  $\text{Na}_2\text{SO}_4$  and concentrated gently below 40 °C under vacuum. The crude residue thus obtained was purified by column chromatography using EtOAc/hexane (2:98), which afforded azidoethane (**2**) as a brown oil, 120 mg (1.69 mmol, 92.0%). IR (neat) ( $\text{cm}^{-1}$ ): 2930, 2867, 1598, 1495, 1467, 1366, 1188, and 1174. <sup>1</sup>H NMR ( $\text{CDCl}_3$ , 300 MHz):  $\delta$  1.74 (3H, t), 3.39 (2H, q). ESI-MS calcd for  $[\text{C}_2\text{H}_5\text{N}_3 + \text{Na}^+]$ : 94.0711; found: 94.0381.

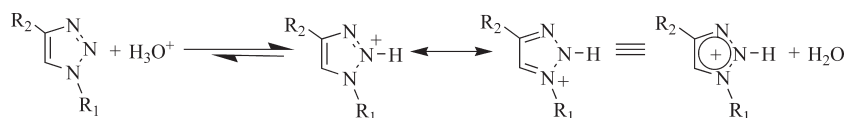
(12) (a) Bhattacharya, S.; Biswas, J. *Langmuir* **2010**, *26*, 4642. (b) Menger, F. M.; Shi, L.; Rizvi, S. A. A. *J. Colloid Interface Sci.* **2010**, *344*, 241. (c) Ahmad, R. K.; Faure, D.; Goddard, P.; Oda, R.; Bassani, D. M. *Org. Biomol. Chem.* **2009**, *7*, 3173. (d) Aimé, C.; Manet, S.; Satoh, S.; Ihara, H.; Park, K.-Y.; Godde, F.; Oda, R. *Langmuir* **2007**, *23*, 12875. (e) Jiao, T.; Liu, M. *Langmuir* **2006**, *22*, 5005. (f) Grinberg, S.; Linder, C.; Kolot, V.; Waner, T.; Wiesman, Z.; Shaubi, E.; Heldman, E. *Langmuir* **2005**, *21*, 7638. (g) Haldar, J.; Aswal, V. K.; Goyal, P. S.; Bhattacharya, S. *Angew. Chem., Int. Ed.* **2001**, *40*, 1228. (h) Bhattacharya, S.; De, S.; Subramanian, M. *J. Org. Chem.* **1998**, *63*, 7640. (i) Bhattacharya, S.; Kumar, V. P. *Langmuir* **2005**, *21*, 71. (j) Bhattacharya, S.; Snehalatha, K.; Kumar, V. P. *J. Org. Chem.* **2003**, *68*, 2741. (k) Bhattacharya, S.; Haldar, J. *Langmuir* **2004**, *20*, 7940. (l) Haldar, J.; Kondaiah, P.; Bhattacharya, S. *J. Med. Chem.* **2005**, *48*, 3823.

(13) Klapotke, T. M.; Rienacker, C. M. *Propellants, Explos., Pyrotech.* **2001**, *26*, 43.



<sup>a</sup> Reagents and conditions: (i), (ii), (iii), and (iv) CuI, DIEA, MeOH, rt, 6–8 h.

**Chart 1**



*1-Azidotetradecane* (**3**). NaN<sub>3</sub> (234 mg, 3.60 mmol) was added to a solution of 1-bromotetradecane (200 mg, 0.72 mmol) in DMF (20 mL) in a round-bottom flask, and the resulting mixture was warmed to 80 °C for 10 h. Then the solvent was evaporated under vacuum to leave a residue, to which EtOAc was added. This afforded an organic layer, which was washed with water (20 mL × 2) and followed by saturated brine (20 mL). Because of the potential explosiveness of azides,<sup>13</sup> the organic layer was dried over anhydrous Na<sub>2</sub>SO<sub>4</sub> and concentrated gently below 40 °C under vacuum. The crude product thus obtained was purified by column chromatography using EtOAc/hexane (2:98) which afforded 1-azidotetradecane (**3**) as a brown oil, 164 mg (0.69 mmol, 95.0%). IR (neat) (cm<sup>-1</sup>): 2930, 2867, and 2104. <sup>1</sup>H NMR (CDCl<sub>3</sub>, 300 MHz): δ 0.78–0.84 (3H, t), 1.18–1.32 (22H, m), 1.64–1.82 (2H, m), 3.30–3.36 (2H, t). ESI-MS calcd for [C<sub>14</sub>H<sub>29</sub>N<sub>3</sub> + Na<sup>+</sup>]: 262.3901; found: 262.2259.

*1,3-Diazidopropane* (**4**). NaN<sub>3</sub> (322 mg, 4.95 mmol) was added to a solution of 1,3-dibromopropane (200 mg, 0.99 mmol) in DMF (5 mL) in a round-bottom flask, and the resulting mixture was warmed gently to 80 °C. After 10 h, the solvent was evaporated under vacuum. The reaction mixture was diluted with EtOAc. The organic layer was washed with water (20 mL × 2) and followed by saturated brine (20 mL). Because of the potential explosiveness of azides,<sup>13</sup> the organic layer was dried over anhydrous Na<sub>2</sub>SO<sub>4</sub> and concentrated under vacuum gently < 40 °C. The residue was

purified by column chromatography (eluent: EtOAc/hexanes, 4:96) to furnish 1,3-diazidopropane (**4**) as a brown oil, 110 mg (0.87 mmol, 88.0%). IR (neat) (cm<sup>-1</sup>): 2924, 2852, and 2100. <sup>1</sup>H NMR (CDCl<sub>3</sub>, 300 MHz): δ 2.26–2.29 (2H, m), 3.30–3.34 (4H, t). ESI-MS calcd for [C<sub>3</sub>H<sub>6</sub>N<sub>6</sub> + Na<sup>+</sup>]: 149.11; found: 149.0552.

*1,3-Diazido-2,2-bis(azidomethyl)propane* (**5**). NaN<sub>3</sub> (169 mg, 2.60 mmol) was added to a solution of 1,3-dibromo-2,2-bis(bromomethyl)propane (200 g, 0.52 mmol) in DMF (5 mL) in a round-bottom flask, and the resulting mixture was warmed slowly to 80 °C. After 10 h of reaction at this temperature, the solvent was evaporated under vacuum. The reaction mixture was diluted with EtOAc. The organic layer was washed with water (20 mL × 2) and followed by saturated brine (20 mL). Because of the potential explosiveness of azides,<sup>13</sup> the organic layer was dried over anhydrous Na<sub>2</sub>SO<sub>4</sub> and concentrated gently under vacuum < 20 °C. The resulting oil was purified by column chromatography (eluent: EtOAc/hexanes, 6:94), which afforded 1,3-diazido-2,2-bis(azidomethyl)propane (**5**) as a colorless solid, 97 mg (0.41 mmol, 80.0%). IR (neat) (cm<sup>-1</sup>): 2923, 2850, and 2099. <sup>1</sup>H NMR (CDCl<sub>3</sub>, 300 MHz): δ 3.27 (8H, s). ESI-MS calcd for [C<sub>5</sub>H<sub>8</sub>N<sub>12</sub> + Na<sup>+</sup>]: 259.1877; found: 259.0893.

*1-Ethyl-1H-[1,2,3]triazol-4-yl-methyl Dodecanoate* (**M1**). Compound **2** (50 mg, 0.70 mmol) was added to a solution of compound **1** (336 mg, 0.70 mmol) in MeOH (6 mL) in a round-bottom flask. After that, *N,N'*-diisopropyl-*N*-ethylamine (DIEA) (452 mg,

3.5 mmol) and CuI (667 mg, 3.5 mmol) were added, and the reaction mixture was stirred for 8 h at room temperature. After 8 h, MeOH was evaporated and the reaction mixture was diluted with  $\text{CHCl}_3$ . The organic layer was washed with saturated aqueous  $\text{KHSO}_4$  solution ( $3 \times 20$  mL), water (20 mL), and saturated brine solution (20 mL). Finally, the organic layer was separated and dried over anhydrous  $\text{Na}_2\text{SO}_4$ . The solvent was removed using a rotary evaporator, and the product was purified by column chromatography over silica gel using a mixture of  $\text{CHCl}_3$  and MeOH [ $v/v = 96:4$ ] to afford a white solid, 158 mg (0.51 mmol, 73.0%). IR (neat) ( $\text{cm}^{-1}$ ): 2924, 2852, 1739, and 1625.  $^1\text{H}$  NMR ( $\text{CDCl}_3$ , 300 MHz):  $\delta$  0.81–0.86 (3H, t), 1.23 (16H, m), 1.81–1.85 (5H, m), 2.23–2.8 (2H, t), 4.24–4.29 (2H, q), 5.14 (2H, s), 7.52 (1H, s). ESI-MS calcd for  $[\text{C}_{17}\text{H}_{31}\text{N}_3\text{O}_2 + \text{Na}^+]$ : 332.4368; found: 332.2314.

*1-Tetradecyl-1H-[1,2,3]triazol-4-yl-methyl Dodecanoate (M2)*. Compound 3 (50 mg, 0.21 mmol) was added to a solution of compound 1 (50 mg, 0.21 mmol) in MeOH (6 mL) in a round-bottom flask. After that, DIEA (136 mg, 1.05 mmol) and CuI (200 mg, 1.05 mmol) were added, and the reaction mixture was stirred for 8 h at room temperature. After 8 h, MeOH was evaporated and the reaction mixture was diluted with  $\text{CHCl}_3$ . The organic layer was washed with saturated  $\text{KHSO}_4$  ( $3 \times 20$  mL), water (20 mL), and saturated brine solution (20 mL). Finally, the organic layer was separated and dried over anhydrous  $\text{Na}_2\text{SO}_4$ . The solvent was removed using a rotary evaporator, and the product was purified by column chromatography over silica gel using a mixture of  $\text{CHCl}_3$  and MeOH [ $v/v = 96:4$ ] to afford a white solid, 78 mg (0.16 mmol, 78.0%). IR (neat) ( $\text{cm}^{-1}$ ): 2929, 2868, 1743, and 1632.  $^1\text{H}$  NMR ( $\text{CDCl}_3$ , 300 MHz):  $\delta$  0.81–0.86 (6H, t), 1.23 (38H, m), 1.85–1.90 (4H, m), 2.27–2.32 (2H, t), 4.29–4.34 (2H, q), 5.19 (2H, s), 7.56 (1H, s). ESI-MS calcd for  $[\text{C}_{29}\text{H}_{55}\text{N}_3\text{O}_2 + \text{Na}^+]$ : 500.7558; found: 500.4192.

*1-[3-(4-Dodecanoyloxymethyl-[1,2,3]triazol-1-yl)-propyl]-1H-[1,2,3]triazol-4-yl-methyl Dodecanoate (D1)*. Compound 4 (50 mg, 0.40 mmol) was added to a solution of compound 1 (191 mg, 0.80 mmol) in MeOH (6 mL) in a round-bottom flask. After that, DIEA (517 mg, 4.00 mmol) and CuI (762 mg, 4.00 mmol) were added, and the reaction mixture was stirred for 8 h at room temperature. After 8 h, solvent was evaporated from the reaction mixture and the residue was dissolved in  $\text{CHCl}_3$ . The organic layer was washed with saturated  $\text{KHSO}_4$  ( $3 \times 20$  mL), water (20 mL), and saturated brine (20 mL). Finally, the organic layer was separated and dried over anhydrous  $\text{Na}_2\text{SO}_4$ . The solvent was removed using a rotary evaporator, and the product was purified by column chromatography over silica gel using a mixture of  $\text{CHCl}_3$  and MeOH [ $v/v = 94:6$ ] to furnish a white solid, 167 mg (0.28 mmol, 70.0%). IR (neat) ( $\text{cm}^{-1}$ ): 2934, 2854, 1726, and 1630.  $^1\text{H}$  NMR ( $\text{CDCl}_3$ , 300 MHz):  $\delta$  0.81–0.86 (6H, t), 1.23 (32H, m), 1.68–1.76 (4H, m), 2.25–2.30 (6H, m), 3.72–3.83 (4H, d), 5.34 (4H, s), 7.26 (2H, s). ESI-MS calcd for  $[\text{C}_{33}\text{H}_{58}\text{N}_6\text{O}_4 + \text{Na}^+]$ : 625.8414; found: 625.4417.

*1-[3-(4-Dodecanoyloxymethyl-[1,2,3]triazol-1-yl)-2,2-bis(4-dodecanoyloxymethyl-[1,2,3]triazol-1-yl-methyl)propyl]-1H-[1,2,3]triazol-4-yl-methyl Dodecanoate (T1)*. Compound 5 (50 mg, 0.21 mmol) was added to a solution of compound 1 (200 mg, 0.84 mmol) in MeOH (6 mL) in a round-bottomed flask. After that, DIEA (543 mg, 4.2 mmol) and CuI (800 mg, 4.2 mmol) were added, and the reaction mixture was stirred for 8 h at room temperature. After 8 h, solvent was evaporated from the reaction mixture and the residue was dissolved in  $\text{CHCl}_3$ . The organic layer was washed with saturated  $\text{KHSO}_4$  ( $3 \times 20$  mL), water (20 mL), and saturated brine (20 mL). Finally, the organic layer was separated and dried over anhydrous  $\text{Na}_2\text{SO}_4$ . The solvent was removed using a rotary evaporator, and the product was purified by column chromatography over silica gel using a mixture of  $\text{CHCl}_3$  and MeOH [ $v/v = 92:8$ ] to furnish a white solid, 166 mg (0.14 mmol, 66.0%). IR (neat) ( $\text{cm}^{-1}$ ): 2936, 2876, 1749, and 1634.  $^1\text{H}$  NMR ( $\text{CDCl}_3$ , 300 MHz):  $\delta$  0.83–0.88 (12H, t), 1.22 (64H, m), 1.52–1.56 (8H, m), 2.23–2.28 (8H, t), 3.67 (8H, s), 5.24 (8H, s),

7.19 (4H, s). ESI-MS calcd for  $[\text{C}_{65}\text{H}_{112}\text{N}_{12}\text{O}_8 + \text{Na}^+]$ : 1212.6506; found: 1211.6624.

**2.3. Computational Studies.** An optimization of the energy-minimized structure of each click chemistry based triazole adduct was performed using Gaussian 98 program and RHF/6-31G\* level of theory.<sup>14</sup> The ball-stick structure of each molecule was drawn using Gauss View software, and then the coordinates of these structures were taken and run in Gaussian 98 to get the optimized geometry. The distance between the “head” to the “tail” carbon atom was determined using ChemCraft software.<sup>15</sup>

**2.4. Aggregate Preparation.** Each adduct was dissolved in chloroform in separate autoclaved glass vial. Thin film was made by evaporation of the organic solvent under a steady stream of dry nitrogen. The last traces of chloroform were removed by keeping the film under vacuum overnight. Freshly autoclaved water (Milli-Q) or particular buffer was added to the individual film such that the final concentration of the adduct was maintained at  $\sim 1$  mM. The mixtures were kept for hydration at  $4^\circ\text{C}$  for 6–8 h and were repeatedly freeze–thawed (ice-cold water to  $70^\circ\text{C}$ ) with intermittent vortexing to ensure optimal hydration. Sonication of these suspensions for 15 min in a bath sonicator at  $70^\circ\text{C}$  afforded approximately spherical aggregates as evidenced from transmission electron microscopy. The aggregates were prepared and kept under sterile conditions. The aggregates were found to be stable even after keeping them for more than 1 month.

**2.5.  $pK_a$  Measurements of Click Adduct Aggregates.** UV–vis spectra of the aggregate of each click adduct in aqueous media or media of different acidities (by adding solutions of  $\text{H}_2\text{SO}_4$ ) were recorded using Shimadzu UV-2100 spectrophotometer at  $25^\circ\text{C}$ . Then the ratios of absorbance maxima before and after protonation of triazole groups in the aggregates of each click adduct of each spectrum were plotted against the pH of the media. The points obtained were fitted (Boltzmann) using Origin 8.0 software, and from the break we obtained the  $pK_a$  value of the aggregates of each click adduct.

**2.6. Dye Entrapment Studies.** Films of a given click adduct were prepared as described above and an appropriate amount of 0.1 mM methylene blue (MB) ( $\lambda_{\text{max}} = 665$  nm) was added such that each click adduct concentration was 5 mM. A 2 mL aliquot of the resulting click adduct suspension was loaded on to a column packed with pre-equilibrated Sephadex G-50. Gel filtration was performed using freshly autoclaved water (Milli-Q) as the eluent until elution of free dye was complete. Neat Triton-X-100 was added to aliquots of fractions to give a 1 wt % concentration of Triton X 100, and the vesicles were lysed by bath sonication of the resulting solution for 2 min at room temperature. The absorbances at 665 nm for all the fractions containing lysed solutions was determined and plotted against the elution volume.

**2.7. Transmission Electron Microscopy.** The aqueous aggregates of the adducts (1 mM) were examined under transmission electron microscopy by negative staining using 0.5% uranyl acetate. A  $10\ \mu\text{L}$  sample of the suspension was loaded onto Formvar-coated, 400 mesh copper grids and allowed to remain for 1 min. Excess fluid was removed from the grids by touching their edges with filter paper, and  $10\ \mu\text{L}$  of 0.1% uranyl acetate was applied on the same grid after which the excess stain was similarly removed from the grids. First, the grids were air-dried, and then the last traces of water were removed under vacuum. The samples were observed under TEM (TECNAI T20) operating at an acceleration voltage (dc voltage) of 100 keV. Micrographs were recorded at a magnification of 10 000–80 000 $\times$ .

**2.8. Dynamic Light Scattering.** Unilamellar vesicles (1 mM) prepared in buffered aqueous media (as mentioned under the aggregate preparation) were diluted to 0.33 mM and were used for dynamic light scattering (DLS) measurements. DLS measurements were performed at room temperature using a Malvern Zetasizer

(14) (a) Kumar, V. P.; Ganguly, B.; Bhattacharya, S. *J. Org. Chem.* **2004**, *69*, 8634.

(b) Bhattacharya, S.; Vemula, P. K. *Org. Chem.* **2005**, *70*, 9677.

(15) Kress, J. W. *J. Phys. Chem. A* **2005**, *109*, 7757.

Nano ZS particle sizer (Malvern Instruments Inc., Westborough, MA). Samples were prepared and examined under dust-free conditions. Mean hydrodynamic diameters reported were obtained from the Gaussian analysis of the intensity-weighted particle size distributions.

**2.9. Differential Scanning Calorimetry.** Thermotropic properties of the adduct aggregate samples in aqueous media were investigated by high-sensitivity DSC using a CSC-4100 model multicell differential scanning calorimeter (Calorimetric Sciences Corp., Lindon, UT). Click adduct aggregate samples were prepared as mentioned under the aggregate preparation. Each click adduct aggregate sample (0.5 mL) in buffered aqueous media (pH 2.0 or 7.4) was carefully transferred into three of the four DSC ampules, and the fourth one was filled with 0.5 mL of buffered aqueous media. Then the ampules were sealed. The measurement was carried out in the temperature range of 20–70 °C at a scan rate of 20 °C/h. At least two consecutive heating and cooling were performed. Baseline thermograms were obtained using same amount of the degassed buffer in the respective DSC cells. The thermograms for the adduct aggregate samples were obtained by subtracting the respective baseline thermogram from the sample thermogram using “CpCalc” software. From the plot of excess heat capacity vs temperature, solid-to-fluid transition temperature ( $T_{s\rightarrow f}$ ), fluid-to-solid transition temperature ( $T_{f\rightarrow s}$ ), and calorimetric enthalpies ( $\Delta H_c$ ) of the transitions were obtained. The size of the cooperativity unit (CU) for the melting transition was determined using the formula  $CU = \Delta H_{vH}/\Delta H_{cal}$ , where the  $\Delta H_{vH}$  is the van't Hoff enthalpy and the  $\Delta H_{cal}$  is the calorimetric enthalpy. The van't Hoff enthalpy was calculated from the equation  $\Delta H_{vH} = 6.9T_m^2/\Delta T_{1/2}$ , where  $T_m$  is the phase transition temperature and  $\Delta T_{1/2}$  is the full width at half-maximum of the thermogram.

**2.10. Measurements of Aggregate Hydration.** Paldan, which is a palmitoyl analogue of Prodan, was synthesized by the procedures of Weber, Davis, and Balter et al. The synthesis of Paldan was performed by following the literature procedure.<sup>16,17</sup> First, 2-methoxynaphthalene was treated by *n*-C<sub>15</sub>H<sub>31</sub>COCl in the presence of AlCl<sub>3</sub> to get 6-palmitoyl-2-methoxynaphthalene. 6-Palmitoyl-2-methoxynaphthalene was then converted to the corresponding dimethylamino derivative (Paldan) by following the appropriate literature procedure.<sup>16,17</sup> After purification and spectral characterizations, the synthetic Paldan was used for spectroscopic studies. All the fluorescence experiments were carried out on sonicated click adduct aggregate samples in aqueous media using adduct-to-probe ratio of 1000:3. The width of the excitation and emission slit was 10 nm. Generalized polarization of emission (GP) was calculated using the equation

$$GP_{em} = \frac{I_{440} - I_{490}}{I_{440} + I_{490}}$$

where  $I_{440}$  and  $I_{490}$  represent the fluorescence intensities at 440 and 490 nm.<sup>18,19</sup> For the GP values reported herein, an excitation wavelength of 350 nm was used. For excitation, the spectra wavelength was kept at 440 nm.

**2.11. Fluorescence Anisotropy Measurements.** For the preparation of click adduct suspensions doped with fluorescent probe, 1,6-diphenylhexatriene (DPH), the probe in dry CHCl<sub>3</sub> was cosolubilized with a given click adduct in chloroform. A thin film was generated upon evaporation of solvent in the dark, and then DPH-doped vesicles (adduct concentration = 1.0 mM) were prepared by the freeze–thaw method followed by sonication as mentioned above. All the fluorescence anisotropy experiments were carried out on sonicated suspensions using an adduct-to-probe

ratio of 1000:4. Steady-state fluorescence anisotropies sensed by DPH-doped suspensions were measured in a HORIBA Jobin Yvon Fluorolog spectrofluorimeter equipped with polarizers upon excitation of DPH at 360 nm. The emission intensity was followed at 430 nm. The slit widths were kept at 5 nm for both the excitation and the emission. The fluorescence intensities of the emitted light polarized parallel ( $I_{VV}$ ) and perpendicular to the excited light ( $I_{VH}$ ) were measured at different temperatures. These fluorescence intensities were corrected for scattered light intensity. The fluorescence anisotropy values ( $r$ ) at each temperature were calculated employing the equation  $r = (I_{VV} - GI_{VH})/(I_{VV} + 2GI_{VH})$ , where  $G$  is the instrumental grating factor. The grating factor,  $G$ , was calculated using the equation  $G = I_{HV}/I_{HH}$ , where  $I_{HV}$  and  $I_{HH}$  represent the fluorescence intensities of vertically polarized and horizontally polarized light, respectively, when a horizontally polarized light was used for the probe excitation. The systemic gel-to-liquid crystalline phase transition temperatures ( $T_m$ ) of each click adduct were calculated from the midpoints of the breaks related to the temperature-dependent anisotropy values.<sup>20a,b</sup>

**2.12. Cast-Film XRD Measurements.** An aqueous aggregates of each adduct (1 mM) was placed on a precleaned glass plate which, upon air-drying, afforded a thin film of the adduct aggregate on the glass plate. X-ray diffraction (XRD) of an individual cast film was performed using the reflection method with a Phillips X-ray diffractometer.<sup>21a–c</sup> The X-ray beam was generated with a Cu anode, and the Cu K $\alpha_1$  beam of wavelength 1.5418 Å was used for the experiments. Scans were performed for  $2\theta$  values up to 18°.

**2.13. Langmuir Monolayer Studies.** Isotherms of the individual click adduct monolayer at the air-buffered aqueous media interface were recorded on a Nima Langmuir trough (Nima Technology, Coventry, England) equipped with computer control. A paper Wilhelmy plate was used as the surface pressure sensor and situated in the middle of the trough. Two barriers compressed or expanded symmetrically at the same velocity from two sides of the trough. Monolayers were obtained by spreading the chloroform solutions of desired volumes on buffer containing subphases. The subphase temperature was maintained at 25 °C. After spreading, 30 min was allowed for solvent evaporation, and the monolayers were then compressed at a rate of 5 mm/min to record isotherms.

### 3. Results and Discussion

Upon hydration followed by bath sonication for 15 min at 70 °C, each adduct having a 1,2,3-triazole unit was found to get dispersed in aqueous media easily. The suspensions formed from the adducts were found to be stable and optically clear suspensions in aqueous buffer solutions. No precipitation or noticeable increase in turbidity was observed even after 1 month when these suspensions were stored at 4 °C under sterile conditions.

**3.1. pK<sub>a</sub> Measurements of Click Adduct Aggregates.** UV–vis spectra of the aggregates of each click adduct prepared in aqueous media of various pH values were recorded at 25 °C. A representative spectral profile for the aggregates of M1 recorded at various pH values is shown in Figure 2A. At pH 7.6, the aggregates M1 showed a peak at 252 nm due to the presence of the triazole moiety.<sup>11b</sup> Progressive decreases in the pH values of the same aggregates resulted in the evolution of a new peak at 284 nm at the expense of the 252 nm peak. This occurred at pH ≤ 3 due to the formation of protonated triazolium moiety. Then the ratios of the absorbance maxima before and after protonation of triazole

(16) Weber, G.; Davis, F. J. *Biochemistry* **1979**, *18*, 3075.

(17) Lakowicz, J. R.; Bevan, D. R.; Maliwal, B. P.; Cherek, H.; Balter, A. *Biochemistry* **1983**, *22*, 5714.

(18) Parasassi, T.; Di Stefano, M.; Loiero, M.; Ravagnan, G.; Gratton, E. *Biophys. J.* **1994**, *66*, 763.

(19) Parasassi, T.; De Stasio, G.; Ravagnan, G.; Rusch, R. M.; Gratton, E. *Biophys. J.* **1991**, *60*, 179.

(20) (a) Lakowicz, J. *Principles of Fluorescence Spectroscopy*, 1st ed.; Plenum Press: New York, 1983. (b) Shinitzky, M.; Barenholtz, Y. *Biochim. Biophys. Acta* **1978**, *525*, 367.

(21) (a) Bhattacharya, S.; Dileep, P. V. *J. Phys. Chem. B* **2003**, *107*, 3719. (b) Kimizuka, N.; Kawasaki, T.; Kunitake, T. *J. Am. Chem. Soc.* **1993**, *115*, 4387. (c) Kimizuka, N.; Kawasaki, T.; Hirata, K.; Kunitake, T. *J. Am. Chem. Soc.* **1998**, *120*, 4094.

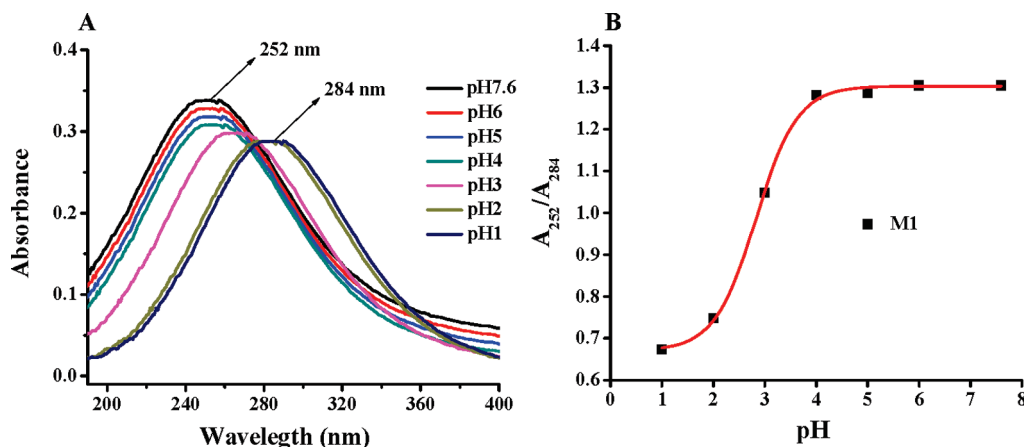


**Figure 2.** (A) UV–vis spectra of the aggregates of click adduct **M1** (conc. = 1 mM) in aqueous buffered media of different pH values. (B) Plot of the ratio of absorbance maxima before and after protonation of triazole groups in the aggregates of click adduct **M1** of each spectrum vs the pH of the media.

**Table 1.** Apparent  $pK_a$  Values of the Aggregates of Each Click Adduct Formed in Aqueous Media<sup>a</sup>

click adduct	$pK_a$
<b>M1</b>	2.9
<b>M2</b>	2.9
<b>D1</b>	3.1
<b>T1</b>	3.1

<sup>a</sup>The  $pK_a$  values were within  $\pm 0.1$  units in duplicate experiments.

groups in the aggregates of each click adduct of each spectrum were plotted against the pH of the media. The points obtained were fitted using Origin 8.0 software, and from the break we obtained the systemic  $pK_a$  value of the adduct aggregates of **M1** (Figure 2B). The  $pK_a$  values of the aggregates of each click adduct including that of **M1** are given in Table 1. The apparent  $pK_a$  values of the aggregates of monomeric click adducts **M1** and **M2** were found to be 2.9 (same for the two adducts), whereas that of the aggregates of click adducts **D1** and **T1** was found to be  $\sim 3.1$ .

**3.2. Aggregate Characterizations.** Upon hydration followed by dispersal by bath sonication for 15 min at 70 °C in freshly autoclaved water (Milli-Q) or a particular buffer, each of the four compounds (1 mM) formed optically clear, stable suspensions. No precipitation or noticeable increase in turbidity was observed even after 1 month when these suspensions were stored at 4 °C under sterile conditions. Examination of freshly prepared aqueous suspensions of each compound by TEM revealed the existence of vesicle-like nanoscopic structures (Figure 3). The dispersions of the dimeric adduct **D1** showed a few elongated nonspherical structures as well, whereas that of the other adducts formed spherical morphologies as evident from the TEM study. Interestingly, the vesicular aggregates were observed from both **M1** (one fatty acid ester-linked chain with a delocalized protonated triazole) and **M2** (one fatty acid ester-linked chain and one  $n\text{-C}_{14}\text{H}_{29}$  chain with a protonated triazole). Observations of vesicle formation from a single-chain systems are not unprecedented. Indeed, vesicle formation from a single-chain compound having a large polar headgroup (not related to the present design) is already reported.<sup>22</sup>

All the adduct suspensions in two buffer media (pH 2 and 7.4) were further characterized using DLS, as shown in Table 2. The hydrodynamic diameter of the aggregates of each click adduct increased modestly with the decrease in the pH of the media. Thus, the protonation of the triazole groups in the aggregates of each click

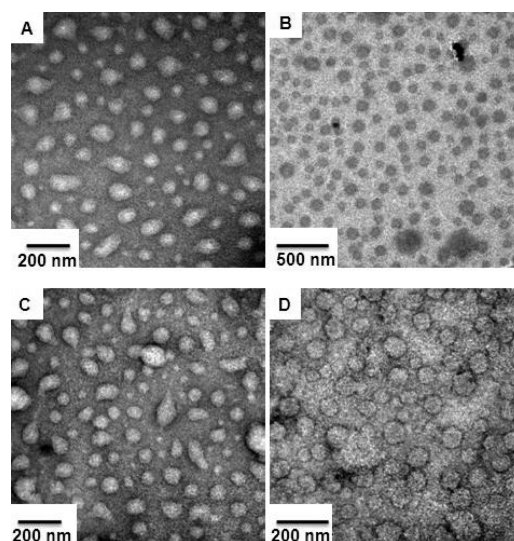


**Figure 3.** Negative-stain transmission electron micrographs of aqueous suspensions of (A) **M1**, (B) **M2**, (C) **D1**, and (D) **T1**.

adduct probably caused a slight increase in the interamphiphilic headgroup repulsion, resulting in an increase in the hydrodynamic diameter. Aggregates of **T1** showed the largest hydrodynamic diameter, whereas that of **D1** showed the smallest hydrodynamic size in both pH values of the buffered aqueous media. Among the monomeric adducts, aggregates of **M1** showed smaller size, which was also evidenced from their TEM images. The sizes of the aggregates obtained from DLS and TEM experiments were not the same but followed an approximately similar trend. The shrinkages in aggregate sizes observed in TEM could be due to drying of the samples—a step required before imaging the micrographs.<sup>23</sup>

A representative optimized molecular structure of **M1** using the RHF/6-31G\* level of theory<sup>25</sup> is shown in Figure 4. Other molecular structures obtained using the same computational method are shown in the Supporting Information (Figure S1). From the optimized structure, we determined the theoretical length of the adduct **M1** by measuring the distance from the “head” carbon atom to the “tail” carbon atom with the help of ChemCraft software. Then the theoretical bilayer width was calculated by

(23) Bhattacharya, S.; Bajaj, A. *Langmuir* **2007**, *23*, 8988.

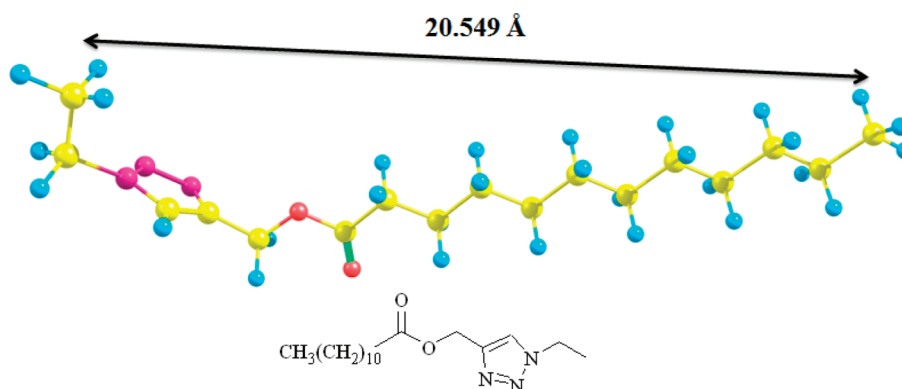
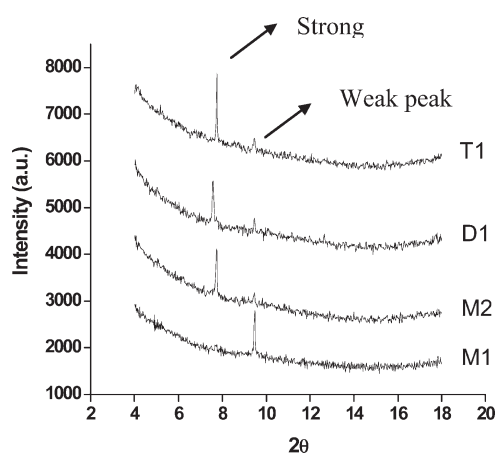
(24) Feng, Z. V.; Spurlin, T. A.; Gewirth, A. A. *Biophys. J.* **2005**, *88*, 2154.

(25) Spelios, M.; Nedd, S.; Matsunaga, N.; Savva, M. *Biophys. Chem.* **2007**, *129*, 137.

**Table 2.** DLS Hydrodynamic Diameters, Sizes from TEM, Thermal Phase Transition Temperatures, and Unit Bilayer Thicknesses of the Click Adduct Aggregates<sup>a</sup>

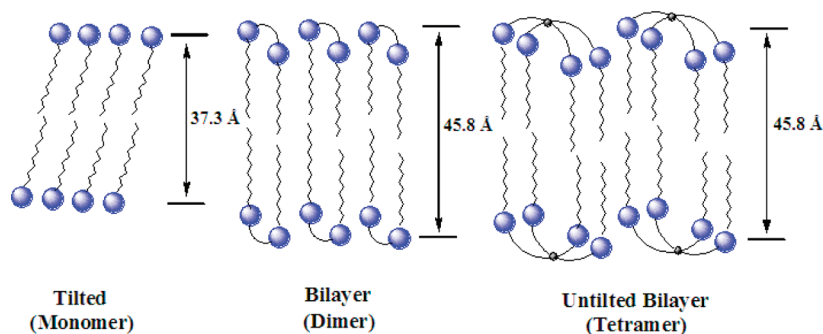
adduct	DLS size <sup>b</sup> ( $\pm 5$ nm)		TEM diameter <sup>c</sup> (nm)	dye entrapment capacity <sup>d</sup> (%)	unit bilayer thickness ( $\text{\AA}$ )	
	pH 2	pH 7.4			obsd <sup>e</sup>	calcd <sup>f</sup>
<b>M1</b>	170	165	80–100	0.97	37.3	41.1
<b>M2</b>	220	210	160–180	1.24	46.6, 37.5 (w)	42.0
<b>D1</b>	145	130	60–80	0.76	45.8, 37.4 (w)	42.1
<b>T1</b>	280	275	140–150	1.52	45.8, 37.4 (w)	40.3

<sup>a</sup> Each aggregate (1 mM) was prepared by sonication (Elma, Transsonic bath T460/H, Germany) for 15 min at 70 °C and at 35 kHz. <sup>b</sup> Dynamic light scattering (DLS) was examined with aqueous suspensions of each adduct prepared under the same conditions. <sup>c</sup> Average sizes of the aggregates obtained from negative stain TEM. <sup>d</sup> [Click adduct] = 5 mM; [methylene blue] = 0.1 mM. <sup>e</sup> As obtained from reflection X-ray diffraction of cast films. <sup>f</sup> Sum of the lengths of two molecular layers in their energy-minimized, fully extended conformation as obtained from theoretical models.

**Figure 4.** Energy-minimized structure of the adducts **M1**, **M2**, **D1**, and **T1** (yellow: C; light blue: H; purple: N; red: O).**Figure 5.** XRD patterns of the cast films obtained from the suspensions of each of the four click chemistry based adducts.

multiplying the monolayer width obtained from the optimized structure by a factor of 2. The bilayer widths of each adduct aggregates were experimentally determined from the cast films obtained by a reported procedure followed by XRD experiments, and the XRD patterns obtained from the cast films of all the four click chemistry based adducts are shown in Figure 5.<sup>26</sup> The bilayer widths of each of the adduct aggregates are given in Table 2.

From the XRD experiments, the  $2\theta$  values for each of the sample were obtained; the bilayer width of each adduct aggregate was obtained from Bragg's equation ( $n\lambda = 2d \sin \theta$ ). Each adduct aggregate showed two peaks under XRD, one strong (in the region 7.55–7.75 of  $2\theta$  values) and the other one weak, except for the monomer **M1**, which showed only one peak at 9.48 of  $2\theta$  value corresponding to the bilayer width of 37.32 Å. One can interpret these data on the basis of formation of slightly tilted bilayer structures in case of **M1** in aqueous media as its bilayer width determined from XRD is less than the theoretical bilayer width determined from its optimized structure (Scheme 3). On the other hand, the adduct aggregates of **M2**, **D1**, and **T1** manifested both

**Scheme 3.** Schematic Representation of Possible Bilayer-Forming Motifs with Various Triazole-Based Adducts

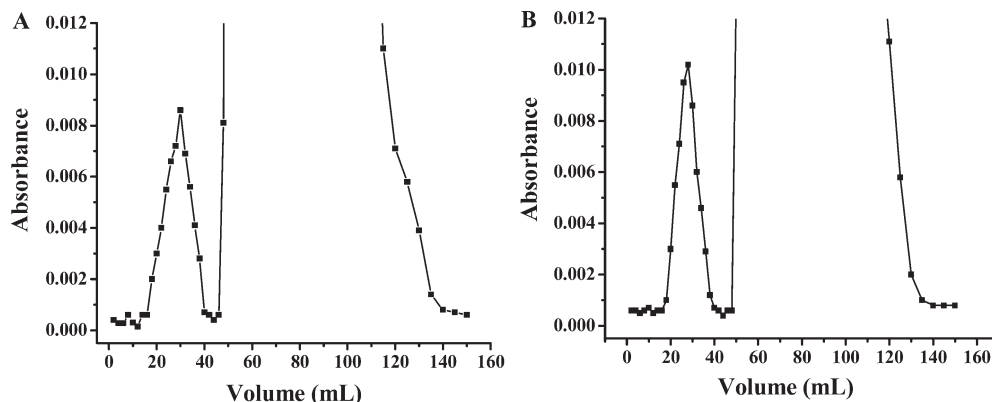


**Figure 6.** Dye entrapment profile of aqueous suspension of (A) **M1** and (B) **T1** in methylene blue (MB). [**M1**] or [**T1**] = 5.0 mM; [MB] = 0.1 mM. The absorbance at 665 nm was checked for all fractions.

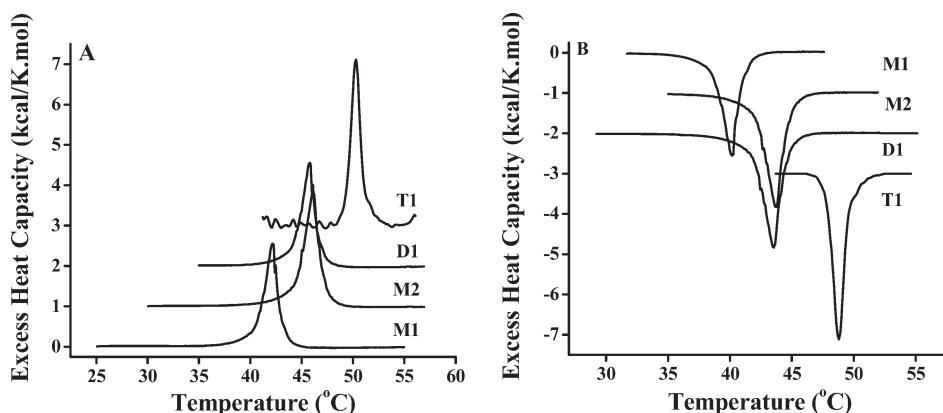


**Figure 7.** (A) Thermotropic phase transitions of various adduct suspensions (1 mM) in buffered aqueous media (pH 7.4) as evidenced by DSC heating scans and (B) cooling scans. Both the thermograms have been successively raised from the baseline by 1 kcal/(K mol) steps for clarity.

regular bilayer structures. The untilted bilayer structures are more prominent for the adduct aggregates of **M2**, **D1**, and **T1** as all of them show strong peaks in the region 9.47–9.49 of  $2\theta$  values corresponding to the bilayer width in the region 45.80–46.65 Å.

**3.2.1. Inner Aqueous Compartments.** To confirm vesicular aggregate formation from these newly synthesized click adducts, we employed dye entrapment studies to examine whether these aggregates contained closed inner aqueous compartments. For instance, the amphiphiles which form micelles in aqueous media do not have the ability to entrap hydrophilic water-soluble molecules (dye). For this purpose, we chose a dye, methylene blue (MB). Gokel et al.<sup>27</sup> showed using this dye that the aggregates of steroidal azacrown derivatives in aqueous media possessed entrapment capacities. To find the entrapment capacities (if any) of the aggregates generated from each click adduct (**M1**, **M2**, **D1**, and **T1**), we made vesicles from each adduct by vortexing followed by sonication for 10 min at 70 °C of the hydrated films to afford a final concentration of 5 mM in water containing 0.1 mM MB. Then freshly autoclaved water (Milli-Q) was used for elution of the gel filtration column (Sephadex G-50), and separate fractions of each were collected. The profile of the gel filtration was obtained by plotting the absorbance at 665 nm of all the fractions obtained from the gel filtration column vs the elution volume. Dye entrapment profile of aqueous suspension of click adducts **M1** and **T1** are shown in Figure 6. In all the cases, it was observed that there was a

small initial portion containing vesicles entrapping approximately 0.76–1.52% of total dye followed by a large peak which was due to the free, unentrapped dye. It is clear that the MB molecules associated with vesicles could be distinctly separated from the free dye. Thus, each click chemistry based adduct formed closed vesicular aggregates with inner aqueous compartments. The percentage of dye entrapment capacity of each vesicular aggregate of a given click adduct is given in Table 2.

### 3.3. Thermal Properties of the Adduct Aggregates.

**3.3.1. Differential Scanning Calorimetry (DSC).** To determine the temperature ( $T_m$ ) at which the phase transition of the individual aggregate from solidlike phase to fluidlike phase takes place,<sup>28</sup> we examined their aqueous suspensions by DSC at pH 7.4 (Figure 7). Each adduct suspension demonstrated sharp chain-melting transitions both during heating and cooling scans. The dependence of the thermotropic phase transition ( $T_m$ ) of various click adduct aggregates at this pH is shown in Figure S3 (Supporting Information). The phase transition temperatures ( $T_m$ ) and other thermotropic parameters as obtained from the DSC studies with each adduct aggregates are given in Table 3.

As the number of long chains in the adducts increased from one to four, the phase transition temperatures also increased from 42.1 to 50.3 °C. The adduct **M1**, which contains only one  $C_{12}$  chain, showed a  $T_m$  at ~42.1 °C, whereas the incorporation of four  $C_{12}$  chains in the adduct **T1** showed the highest  $T_m$  at ~50.3 °C. The adducts **M2** and **D1** which contain two  $C_{12}$  chains showed  $T_m$  at

(26) Bhattacharya, S.; Bajaj, A. *J. Phys. Chem. B* **2007**, *111*, 13511.

(27) DeWall, S. L.; Wang, K.; Berger, D. R.; Watanabe, S.; Hernandez, J. C.; Gokel, G. W. *J. Org. Chem.* **1997**, *62*, 6784.

(28) De, S.; Aswal, V. K.; Goyal, P. S.; Bhattacharya, S. *J. Phys. Chem.* **1996**, *100*, 11664.

~46.0 and 45.8 °C, respectively. The other thermal transition parameters, e.g., transition enthalpy ( $\Delta H_c$ ) and entropy rise as one moves from **M1** to **D1** to **T1**, which is consistent with the increase in the number of their hydrocarbon chains. Between **M1** and **M2**, the same trend is seen as **M2** is significantly more hydrophobic (two hydrocarbon chains and one triazole headgroup) than the other monomeric adduct, **M1**. It appears the dimer **D1** is slightly less hydrophobic (two long chains and two triazole head groups) compared to **M2**, and consistently its thermal parameters were lower than that of **M2**. The corresponding cooperativity units of the thermal transition of the adducts followed similar trends. The transition of aggregates of the tetrameric **T1**, which contains four long chains and four triazole units, was found to be the most cooperative among the aggregates of each type of adduct.

Further we performed the DSC experiments with the click adduct aggregates prepared at pH 2.0. We did not observe any significant changes in the thermal phase transition temperatures using DSC of the aggregates of each click adduct. This confirms again that the protonation of the triazole groups in the aggregates of the click adduct did not influence the packing and the  $T_m$  values in any significant way. The DSC thermogram plots at pH 2.0 are included in the Supporting Information (Figure S2).

**3.3.2. Polarity of the Click Adduct Aggregates.** The apparent hydration of the adduct aggregates was determined by studying a steady-state fluorescence emission of a polarity sensitive fluorophore, Paldan,<sup>15,16</sup> which is the palmitoyl derivative of the much studied polarity sensitive fluorophore, Prodan. As the chain length of the adducts match approximately with the chain length of Paldan, the fluorophore is expected to report the hydration of the present set of adduct aggregates correctly. Paldan was found to be highly sensitive to the polarity of the surrounding medium.

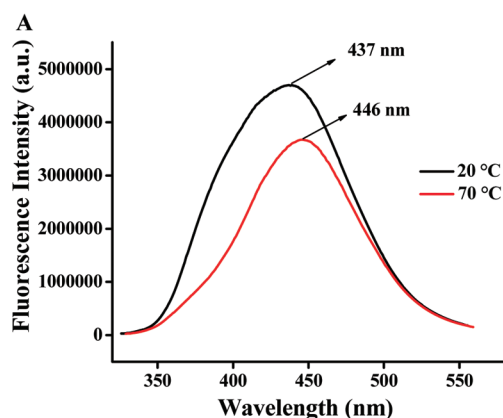
**Table 3. Thermotropic Parameters As Obtained from DSC Studies with Various Click Adduct Aggregates (1 mM) in Buffered Aqueous Media (pH 7.4)**

adduct	$T_m^a$ (°C)		$\Delta H_c^b$ (kcal/mol)		$\Delta S_c^c$ (cal/(K mol))		C.U. <sup>d</sup>
	up scan	down scan	up scan	down scan	up scan	down scan	
<b>M1</b>	42.1	40.2	5.6	5.7	19	22	37
<b>M2</b>	46.0	43.7	8.3	8.8	34	37	56
<b>D1</b>	45.8	43.5	6.4	6.9	23	26	46
<b>T1</b>	50.3	48.8	14.8	14.1	44	40	81

<sup>a</sup> Accuracy of  $T_m$  was  $\pm 0.2$  °C between successive runs of the same sample; two different sample preparations gave a difference of  $\pm 1.0$  °C.

<sup>b</sup> Values were within  $\pm 0.2$  kcal/mol. <sup>c</sup> Values varied within  $\pm 2$  cal/(K mol).

<sup>d</sup> Size of the cooperativity unit.



The adduct aggregates containing 1,2,3-triazole moieties showed  $\lambda_{em}$  in the range of 435–443 nm in their gel states, but in their fluid-melted states, the range of  $\lambda_{em}$  was between 436 and 450 nm (Figure 8A). This change in the emission  $\lambda_{max}$  of the adduct aggregates from the solidlike states to the fluid-melted states is caused due to the increase in the temperature, when a large number of water molecules penetrate inside the adduct aggregates (loosening of the aggregates at higher temperature), and hence there is a bathochromic shift in the emission  $\lambda_{max}$  of the adduct aggregates.

The excitation  $\lambda_{max}$ 's of Paldan in these adduct aggregates in their solid and in the fluid phase are given in Table 4. This further confirms the fact that the emission characteristics of Paldan in these novel triazole-based adduct aggregates are purely due to the excess solvent (water)-mediated stabilization of the excited state. In the solid state (20 °C), the monomer **M1** has the lowest GP value and the tetramer **T1** has highest GP value, whereas the monomer **M2** has larger GP value than that of the dimer **D1** (Supporting Information, Figure S4). So, in the solid state, the tetramer **T1** is the least hydrated among all the four adducts, whereas the aggregate of monomer **M1** is the most hydrated. But in the fluid-melted states, the dimer **D1** is the most hydrated one (lowest GP value), whereas the tetramer **T1** is the least hydrated. From this experiment, we also determined the apparent phase transition temperature from the break in the generalized polarization (GP) vs temperature plot (Figure 8B). The aggregate of monomer **M1** showed the least  $T_m$  value as it contains only one long chain ( $C_{12}$  chain) attached to the triazole moiety, whereas that of the tetramer **T1** showed the highest  $T_m$  value as it contains four  $C_{12}$  chains.

**3.3.3. Fluorescence Anisotropy.** To further understand the thermally induced order-to-disorder transitions in the aggregates formed by each of these four adducts in buffered aqueous media (pH 7.4), the hydrocarbon chain melting were also measured by

**Table 4. Summary of Fluorescence Characteristics of Paldan in Click Adduct Aggregates (1 mM)**

adduct	$\lambda_{ex}^a$ (nm)		$\lambda_{em}^b$ (nm)		GP		$T_m^c$ (°C)
	20 °C	70 °C	20 °C	70 °C	20 °C	70 °C	
<b>M1</b>	355.4	349.6	435.8	436.2	0.205	0.183	41.6
<b>M2</b>	373.6	373.2	440.0	445.2	0.215	0.183	46.9
<b>D1</b>	376.6	375.0	442.8	449.2	0.212	0.180	46.1
<b>T1</b>	378.4	378.2	437.4	446.0	0.219	0.187	49.3

<sup>a</sup> Probe was excited at 350 nm. <sup>b</sup> Emission was monitored at 440 nm.

<sup>c</sup> These values were within  $\pm 0.5$  °C.

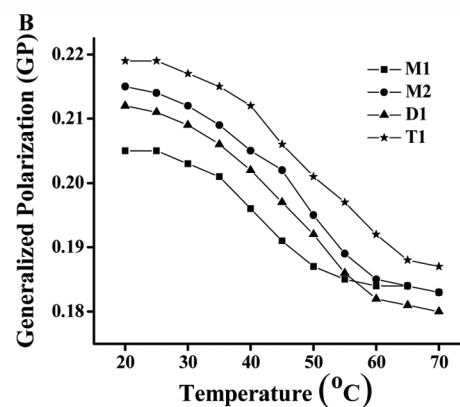


**Figure 8.** (A) Fluorescence emission of Paldan doped in adduct suspension of **T1** in solid (20 °C) and in fluid-melted states (70 °C). (B) Changes in the generalized polarization (GP) of Paldan-doped aggregates (1 mM) of all the four adducts as a function of temperature.

determining the fluorescence anisotropy ( $r$ ) of DPH-doped adducts as a function of temperature. The  $r$  vs  $T$  profiles in Figure 9 show systemic breaks related to the main-chain thermotropic phase transition processes for the individual adduct aggregates. The phase transition temperatures ( $T_m$ ) of all adduct aggregates observed in this study are consistent with the results obtained using DSC. A summary of the thermal order-to-disorder transition parameters as obtained from the steady-state anisotropy experiment due to DPH doped in various click adduct aggregates is given in Table 5.

In this study, we observed that in solid state (20 °C) the adduct **M1** doped with DPH has the highest fluorescence anisotropy ( $r$ ) value (0.243), whereas the adduct **T1** has the lowest  $r$  value (0.226). This suggests that the monomer **M1** is tightly packed in the aggregates in their solid state, but the tetramer

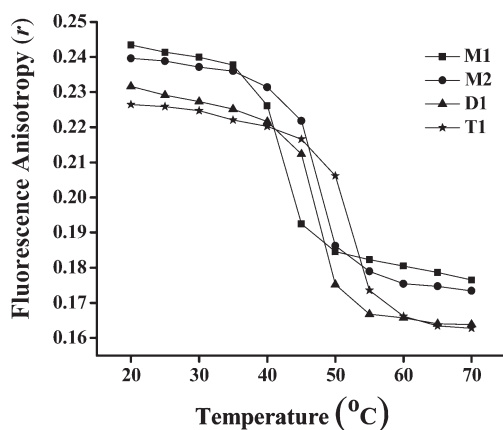


**Figure 9.** Fluorescence anisotropy of DPH-doped adduct aggregates of each of the four adducts in buffered aqueous media (pH 7.4) as a function of temperature.

**Table 5. Thermal Phase Transition Parameters As Obtained from the Steady-State Anisotropy Measurements of the DPH Doped in Click Adduct Aggregates (1 mM)**

adducts	fluorescence anisotropy		$T_m^a$ (°C)
	$r_{20}$	$r_{70}$	
<b>M1</b>	0.243	0.176	42.3
<b>M2</b>	0.239	0.173	47.1
<b>D1</b>	0.232	0.164	47.0
<b>T1</b>	0.226	0.163	51.8

<sup>a</sup> Accuracy of  $T_m$  values were within  $\pm 0.5$  °C.

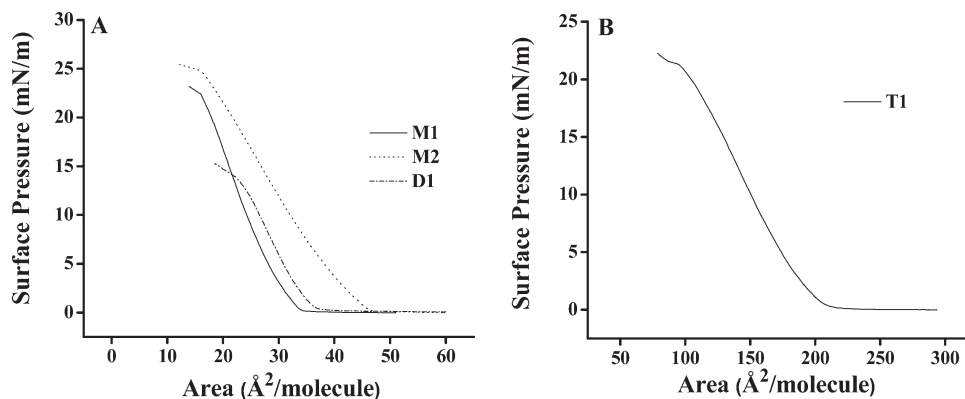


**Figure 10.** Surface pressure–mean molecular area isotherms of click chemistry based adducts at 25 °C spread on buffered aqueous media (pH 7.4). Monolayers at the air–water interface were compressed at a constant rate of 5 mm/min. (A) Adducts **M1**, **M2**, and **D1** and (B) adduct **T1**.

**T1** is relatively loosely packed in the aggregates under analogous conditions. This could be due to the fact that **M1** has only one long chain, whereas **T1** has four long chains and four triazoles in the same structure, so to fit into aggregate an element of “disorderness” in **T1** is manifested more compared to the other adducts in aqueous media. Again the adducts **M2** and **D1** have two long chains, so the disorder in their packing is more compared to that of adduct **M1** as the  $r$  values of **M2** and **D1** (0.239 and 0.232, respectively) are less than that of adduct **M1**. In fluid-melted state (70 °C), again **M1** has the highest  $r$  value (0.176), whereas **T1** has the lowest  $r$  value (0.163), which explains that in the fluid-melted state also the disorder in packing is more in the aggregates of adduct **T1** compared to that of the other adducts.

We also performed the fluorescence anisotropy experiments at pH 2.0 with the click adduct aggregates. We did not, however, observe any noticeable changes in the anisotropy values and in the breaks related to  $T_m$  values in the thermotropic phase transition temperature measurements using the DPH-doped aggregates of each click adduct. This confirms that protonation of triazole groups in the aggregates of each click adduct did not affect the packing and thermotropic phase transition temperature in any major way. Fluorescence anisotropy vs  $T$  plots at pH 2.0 are included in the Supporting Information (Figure S5).

**3.4. Langmuir–Blodgett Monolayer Studies.** Investigating the interfacial properties of the click chemistry based four adducts should be useful as it can provide pertinent information on the interactions occurring between these adducts in their aggregates. The surface properties of each adduct at the air–water interface were studied at 25 °C using the Langmuir film balance technique. Comparisons were also made using water subphase made of two pH values in buffered aqueous media. Data have been presented as a compression isotherm of surface pressure as a function of the mean molecular area and reveal details about the adduct monolayers such as states of order, two-dimensional phase transitions, collapse areas, and collapse pressures.

The monolayer of monomer **M1** collapsed approximately at a surface pressure and mean molecular area (collapse area) of 22.43 mN/m and 15.92 Å<sup>2</sup>, respectively (Figure 10A). The breaks from liquid-expanded phase to liquid-condensed phase were not sharp enough for all the four click adducts. The monolayers of the adducts **M2**, **D1**, and **T1** have relatively sharper breaks from their liquidlike phases to the solidlike phases. For each of the four adducts, the lift of area (i.e., a break from gaslike phase to liquidlike phase) were not the

**Table 6. Isotherm Properties for Click Adducts Obtained at the Air–Liquid Interface on Buffered Aqueous (pH 2.0 and 7.4) Subphases at 25 °C**

adduct	lift-off area ( $\text{\AA}^2$ )		collapse area ( $\text{\AA}^2$ )		collapse pressure (mN/m)	
	pH 2.0	pH 7.4	pH 2.0	pH 7.4	pH 2.0	pH 7.4
<b>M1</b>	32.4	34.8	11.8	15.9	22.4	22.4
<b>M2</b>	41.6	47.4	11.6	15.9	24.3	24.8
<b>D1</b>	34.6	38.3	17.5	22.5	13.9	13.8
<b>T1</b>	202.9	217.1	87.1	94.3	20.4	21.4

same. The adduct **T1** has the highest lift of area ( $217.12 \text{ \AA}^2$ ), so we represent the surface pressure–mean molecular area isotherm plot of adduct **T1** separately from the others (Figure 10B). The lift of areas of adducts **M1**, **M2**, and **D1** are respectively 34.85, 47.38, and  $38.28 \text{ \AA}^2$ . The monolayer of adduct **T1** collapsed at a mean molecular area of  $94.33 \text{ \AA}^2$  (at a surface pressure of 21.35 mN/m), which is highest among all the four adducts. The collapse of the monolayers of the adducts **M1**, **M2**, and **D1** occurs at a mean molecular area of 15.92, 15.98, and  $22.47 \text{ \AA}^2$ , respectively. From this surface pressure–mean molecular area isotherm studies, it may be concluded that the adduct **T1** has the highest headgroup area among the four adducts. Among the monomers, **M1** has higher headgroup area. Isotherm properties of each click adduct obtained at the air–liquid interface on buffered aqueous media (pH 2.0 and 7.4) subphases at 25 °C are given in Table 6.

We observed almost the same collapse area for **M1** and **M2** as both of them contain only one triazole moiety (as headgroup). In **M2**, the second long chain most likely folds back and behaves like a double-chain compound. As the adduct **D1** contains two triazole moieties, so its collapse area is more compared to that of the monomeric counterparts (**M1** and **M2**) but not quite as large as one would expect from two “headgroups”. A possible explanation for the lower collapse area may be due to the partial water solubility of these adducts (**M1**, **M2**, and **D1**) in aqueous media causing a diving down into the subphase during the compression of the films. As the adduct **T1** contains four long chains and four triazole rings within the same molecule, **T1** acts differently during monolayer formation in aqueous media. Hence, we observed a significantly higher collapse area for **T1** as expected in Langmuir monolayer studies.

We also performed Langmuir film formation with the above click adducts at pH 2.0. Consistent with the previous observations, we did not observe major changes in the monolayer film formation at the air–water interface due to each click adduct. This confirms again that protonation of the triazole groups in the aggregates of each click adduct did not remarkably alter the isotherm properties in any significant way. Surface pressure–mean molecular area isotherms of click chemistry based adducts at pH 2.0 are included in the Supporting Information (Figure S6).

## 4. Conclusions

In conclusion, we have synthesized four simple but new 1,2,3-triazole adducts using click chemistry, which on sonic dispersal in aqueous media afforded vesicular aggregates as evidenced from dye entrapment, TEM, and DLS studies. Dye entrapment studies confirmed that each click chemistry based adduct formed closed vesicular aggregates with inner aqueous compartments. XRD experiments with their cast films of the aqueous suspensions indicate the formation of a tilted bilayer type arrangement for the aggregates of **M1**, whereas regular bilayer structures are predominant for the aggregates derived from each of **M2**, **D1**, and **T1**. Recording of UV–vis spectra at various pH values afforded the apparent  $pK_a$  values of each click adduct aggregates. The aggregates of monomeric click adducts (**M1** and **M2**) possess slightly lower  $pK_a$  value than that of the aggregates of dimeric (**D1**) and tetrameric (**T1**) analogues, and the values lie within the range of 2.9–3.1. The hydrodynamic diameter of the aggregates of each click adduct increased modestly with a decrease in the pH of the media. The temperature-induced order-to-disorder transitions of the vesicles and the accompanying changes in hydration were examined using fluorescence anisotropy and generalized polarization measurements with the aid of membrane-soluble probes, DPH and Paldan, respectively. In the solid state, **M1** remains as the most hydrated species, whereas in the fluid-melted phase, **D1** maintains as the most hydrated aggregate. Clearly simple changes in the adduct molecular architecture bring about significant variation in their packing in aggregates and also the hydration of the resulting vesicles. These results are in agreement with the calorimetric data obtained with each of the suspensions. Langmuir monolayer studies confirmed that these click adducts form stable monolayers as well on buffered aqueous subphase at the air–water interface. The mean molecular areas (collapse areas) from the Langmuir monolayer studies were derived from the monolayer studies, and as perhaps expected the adduct **T1** possess the highest headgroup area.

Thus, these click chemistry based simple triazole adducts, which can be very easily prepared, are good candidates for further investigations involving syntheses of novel self-assembling structures. Such adducts when suitably tailored may find wide-ranging applications as novel nanocapsules<sup>29</sup> or in gene delivery.<sup>30</sup> Work is now underway toward this direction in our laboratory.

**Acknowledgment.** J.B. thanks the CSIR, New Delhi, for the award of senior research fellowship.

**Supporting Information Available:** Figures S1–S6 and Table S1. This material is available free of charge via the Internet at <http://pubs.acs.org>.

(29) Yan, X.; He, Q.; Wang, K.; Duan, L.; Cui, Y.; Li, J. *Angew. Chem., Int. Ed.* **2007**, *46*, 2431.

(30) Bhattacharya, S.; Bajaj, A. *Chem. Commun.* **2009**, 4632.